J|A|C|S
ARTICLES

Published on Web 03/10/2010

Cryoreduction of the NO-Adduct of Taurine:α-Ketoglutarate Dioxygenase (TauD) Yields an Elusive {FeNO}^{8} Species

Shengfa Ye,[†] John C. Price,[‡,||] Eric W. Barr,[‡] Michael T. Green,[§] J. Martin Bollinger, Jr.,*[,‡,§] Carsten Krebs,*[,‡,§] and Frank Neese*[,†]

Institute of Physical and Theoretical Chemistry, Universität Bonn, D-53115 Bonn, Germany, and Department of Biochemistry and Molecular Biology, and Department of Chemistry, The Pennsylvania State University, University Park, Pennsylvania 16802

Received November 17, 2009; E-mail: neese@thch.uni-bonn.de; ckrebs@psu.edu; jmb21@psu.edu

Abstract: The Fe(II)- and α-ketoglutarate (αKG)-dependent enzymes are a functionally and mechanistically diverse group of mononuclear nonheme-iron enzymes that activate dioxygen to couple the decarboxylation of αKG, which yields succinate and CO_2, to the oxidation of an aliphatic C−H bond of their substrates. Their mechanisms have been studied in detail by a combination of kinetic, spectroscopic, and computational methods. Two reaction intermediates have been trapped and characterized for several members of this enzyme family. The first intermediate is the C−H-cleaving Fe(IV)−oxo complex, which exhibits a large deuterium kinetic isotope effect on its decay. The second intermediate is a Fe(II):product complex. Reaction intermediates proposed to occur before the Fe(IV)−oxo intermediate do not accumulate and therefore cannot be characterized experimentally. One of these intermediates is the initial O_2 adduct, which is a {FeO_2}^{8} species in the notation introduced by Enemark and Feltham. Here, we report spectroscopic and computational studies on the stable NO-adduct of taurine:αKG dioxygenase (TauD), termed TauD−{FeNO}^{7}, and its one-electron reduced form, TauD−{FeNO}^{8}. The latter is isoelectronic with the proposed O_2 adduct and was generated by low-temperature γ-irradiation of TauD−{FeNO}^{7}. To our knowledge, TauD−{FeNO}^{8} is the first paramagnetic {FeNO}^{8} complex. The detailed analysis of experimental and computational results shows that TauD−{FeNO}^{8} has a triplet ground state. This has mechanistic implications that are discussed in this Article. Annealing of the triplet {FeNO}^{8} species presumably leads to an equally elusive {FeHNO}^{8} complex with a quintet ground state.

Introduction

The Fe(II)- and α-ketoglutarate(αKG)-dependent enzymes represent a large and functionally diverse family of enzymes[1] that catalyze steps in, among other processes, the biosyntheses of antibiotics[2] and collagen,[3] the repair of alkylated DNA,[4] the detection of and response to oxygen insufficiency (hypoxia),[5] and the regulation of gene expression.[6] They couple the reductive activation of dioxygen to the oxidation of their substrates and the decarboxylation of the cosubstrate, αKG, to succinate. In most of the reactions, the substrate is hydroxylated, but other outcomes, including desaturation, cyclization, and halogenation, also occur.[1a−c,7] In each case, the reaction is carried out at a mononuclear nonheme iron center, which (with the exception of the absence of the carboxylate ligand in the halogenases[7b]) is always facially coordinated by a conserved $(His)_2$−(Asp/Glu)-motif from the protein.[8]

It is commonly accepted that these enzymes follow a conserved chemical mechanism, which was formulated more than 20 years ago by Hanauske-Abel and Günzler.[9] The proposed mechanism is shown in Scheme 1.[1]

[†] Universität Bonn.
[‡] Department of Biochemistry and Molecular Biology, The Pennsylvania State University.
[§] Department of Chemistry, The Pennsylvania State University.
[||] Present address: Institute of Neurodegenerative Diseases, University of California at San Francisco, San Francisco, CA 94143.

(1) (a) Solomon, E. I.; Brunold, T. C.; Davis, M. I.; Kemsley, J. N.; Lee, S.-K.; Lehnert, N.; Neese, F.; Skulan, A. J.; Yang, Y.-S.; Zhou, J. *Chem. Rev.* **2000**, *100*, 235–349. (b) Costas, M.; Mehn, M. P.; Jensen, M. P.; Que, L., Jr. *Chem. Rev.* **2004**, *104*, 939–986. (c) Hausinger, R. P. *Crit. Rev. Biochem. Mol. Biol.* **2004**, *39*, 21–68. (d) Bollinger, J. M., Jr.; Price, J. C.; Hoffart, L. M.; Barr, E. W.; Krebs, C. *Eur. J. Inorg. Chem.* **2005**, *2005*, 4245–4254.
(2) Kershaw, N. J.; Caines, M. E. C.; Sleeman, M. C.; Schofield, C. J. *Chem. Commun.* **2005**, 4251–4263.
(3) (a) Hutton, J. J., Jr.; Tappel, A. L.; Udenfriend, S. *Biochem. Biophys. Res. Commun.* **1966**, *24*, 179–184. (b) Kivirikko, K. I.; Myllyharju, J. *Matrix Biol.* **1998**, *16*, 357–368.
(4) (a) Trewick, S. C.; Henshaw, T. F.; Hausinger, R. P.; Lindahl, T.; Sedgwick, B. *Nature* **2002**, *419*, 174–178. (b) Falnes, P. Ø.; Johansen, R. F.; Seeberg, E. *Nature* **2002**, *419*, 178–182.
(5) (a) Ivan, M.; Kondo, K.; Yang, H.; Kim, W.; Valiando, J.; Ohh, M.; Salic, A.; Asara, J. M.; Lane, W. S.; Kaelin, W. G., Jr. *Science* **2001**, *292*, 464–468. (b) Jaakkola, P.; Mole, D. R.; Tian, Y.-M.; Wilson, M. I.; Gielbert, J.; Gaskell, S. J.; von Kriegsheim, A.; Hebestreit, H. F.; Mukherji, M.; Schofield, C. J.; Maxwell, P. H.; Pugh, C. W.; Ratcliffe, P. J. *Science* **2001**, *292*, 468–472. (c) Epstein, A. C. R. *Cell* **2001**, *107*, 43–54. (d) Bruick, R. K.; McKnight, S. L. *Science* **2001**, *294*, 1337–1340. (e) Yu, F.; White, S. B.; Zhao, Q.; Lee, F. S. *Proc. Natl. Acad. Sci. U.S.A.* **2001**, *98*, 9630–9635. (f) Masson, N.; Willam, C.; Maxwell, P. H.; Pugh, C. W.; Ratcliffe, P. J. *EMBO J.* **2001**, *20*, 5197–5206. (g) Lando, D.; Peet, D. J.; Whelan, D. A.; Gorman, J. J.; Whitelaw, M. L. *Science* **2002**, *295*, 858–861. (h) Hewitson, K. S.; McNeill, L. A.; Riordan, M. V.; Tian, Y.-M.; Bullock, A. N.; Welford, R. W.; Elkins, J. M.; Oldham, N. J.; Bhattacharya, S.; Gleadle, J. M.; Ratcliffe, P. J.; Pugh, C. W.; Schofield, C. J. *J. Biol. Chem.* **2002**, *277*, 26351–26355.

Scheme 1. Proposed Mechanism of the Fe(II)- and α-Ketoglutarate-Dependent Dioxygenases

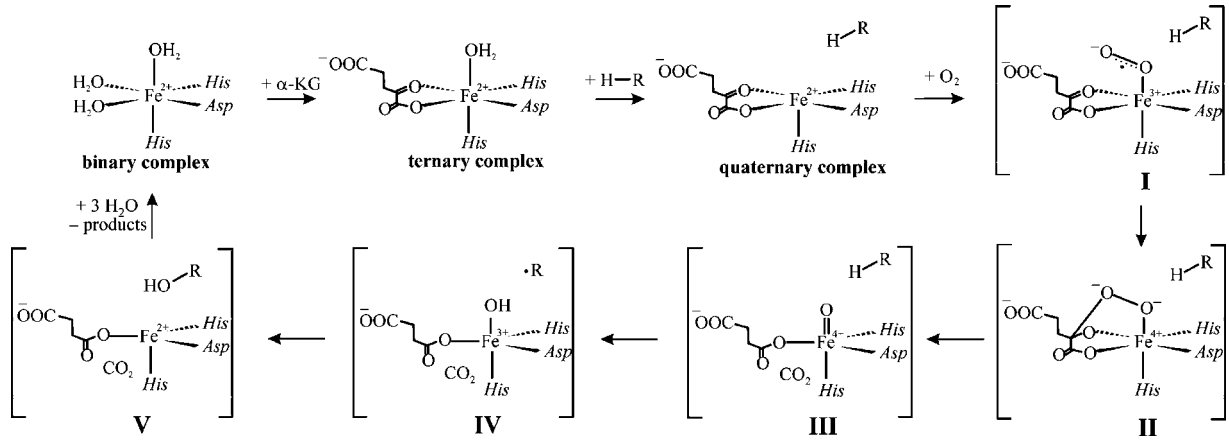

Key features of this mechanism involve (1) addition of dioxygen to the square pyramidal quaternary enzyme:Fe(II):αKG:substrate complex to yield **I**, (2) attack of the uncoordinated O-atom in the O_2-moiety on C2 of αKG to form the bicyclic intermediate **II**, (3) cleavage of the O−O bond and decarboxylation resulting in the Fe(IV)−oxo species **III**, (4) abstraction of an H-atom from the substrate to yield **IV**, (5) hydroxylation via OH rebound,[10] and (6) dissociation of the products and rebinding of the substrate and cosubstrate.

Although this mechanism had been supported by a large number of experimental studies (see ref 1a−c and references cited therein), prior to 2003 none of the proposed intermediates following the addition of oxygen had been directly detected. Investigations on taurine:αKG dioxygenase (TauD) led to the detection of two accumulating, kinetically competent intermediates upon reaction of the TauD:Fe(II):αKG:taurine complex with O_2.[11] A combination of Mössbauer and EPR spectroscopies revealed that the first intermediate, which was termed **J**, contains an Fe ion in the +IV oxidation state and the unusual high-spin ($S = 2$) configuration.[11,12] Demonstration of a large substrate deuterium kinetic isotope effect (^{2}H-KIE) on decay of **J** of ∼50 proved that it is the C−H-cleaving intermediate.[13,14] In the consensus mechanism, this species is an Fe(IV)−oxo (ferryl) complex (**III**). The presence of the ferryl unit in **J** was subsequently demonstrated by resonance Raman[15] and X-ray absorption spectroscopies.[16] Whereas the results provided definitive proof for the presence of the ferryl unit in **J**, they could not reveal other important structural features, such as the number, identity, and disposition of ligands in the Fe(IV) coordination sphere. To probe these important structural features, a series of models for **J** have been evaluated by density functional theory (DFT) calculations. Calculations of spectroscopic parameters (Mössbauer isomer shift, quadrupole splitting, and asymmetry parameter, ^{57}Fe hyperfine coupling tensor, and zero field splitting (ZFS) parameters, *D* and *E*/*D*) allowed us to differentiate various models. The calculated parameters of distorted octahedral models for **J**, in which one of the carboxylates serves as a monodentate ligand and the other as a bidentate ligand, and a trigonal bipyramidal model, in which both carboxylates serve as monodentate ligands, agree well with the experimental parameters, whereas the calculated parameters of a square pyramidal model, in which the oxo ligand is in the equatorial plane, are inconsistent with the data.[17] This work lends credence to the idea that the combination of Mössbauer spectroscopy and DFT calculations can provide detailed structural information for reactive intermediates in the catalytic cycles of iron enzymes. Fe(IV) intermediates with similar spectroscopic parameters, which presumably are all Fe(IV)−oxo species, have been trapped in several other mononuclear nonheme enzymes.[18]

The second intermediate state that accumulates is a Fe(II)-containing product complex.[18a,c,19] States preceding the C−H-cleaving Fe(IV)−oxo intermediate, that is, the proposed Fe(III)−superoxo complex, **I**, and the bicyclic peroxyhemiketal,

(6) (a) Tsukada, Y.-i.; Fang, J.; Erdjument-Bromage, H.; Warren, M. E.; Borchers, C. H.; Tempst, P.; Zhang, Y. *Nature* **2006**, *439*, 811–816. (b) Cloos, P. A. C.; Christensen, J.; Agger, K.; Maiolica, A.; Rappsilber, J.; Antal, T.; Hansen, K. H.; Helin, K. *Nature* **2006**, *442*, 307–311. (c) Klose, R. J.; Yamane, K.; Bae, Y.; Zhang, D.; Erdjument-Bromage, H.; Tempst, P.; Wong, J.; Zhang, Y. *Nature* **2006**, *442*, 312–316.
(7) (a) Vaillancourt, F. H.; Yin, J.; Walsh, C. T. *Proc. Natl. Acad. Sci. U.S.A.* **2005**, *102*, 10111–10116. (b) Blasiak, L. C.; Vaillancourt, F. H.; Walsh, C. T.; Drennan, C. L. *Nature* **2006**, *440*, 368–371.
(8) (a) Que, L., Jr. *Nat. Struct. Biol.* **2000**, *7*, 182–184. (b) Koehntop, K. D.; Emerson, J. P.; Que, L., Jr. *J. Biol. Inorg. Chem.* **2005**, *10*, 87–93.
(9) Hanauske-Abel, H. M.; Günzler, V. *J. Theor. Biol.* **1982**, *94*, 421–455.
(10) Groves, J. T.; McClusky, G. A. *J. Am. Chem. Soc.* **1976**, *98*, 859–861.
(11) Price, J. C.; Barr, E. W.; Tirupati, B.; Bollinger, J. M., Jr.; Krebs, C. *Biochemistry* **2003**, *42*, 7497–7508.
(12) Krebs, C.; Price, J. C.; Baldwin, J.; Saleh, L.; Green, M. T.; Bollinger, J. M., Jr. *Inorg. Chem.* **2005**, *44*, 742–757.
(13) Price, J. C.; Barr, E. W.; Glass, T. E.; Krebs, C.; Bollinger, J. M., Jr. *J. Am. Chem. Soc.* **2003**, *125*, 13008–13009.
(14) Bollinger, J. M., Jr.; Krebs, C. *J. Inorg. Biochem.* **2006**, *100*, 586–605.
(15) (a) Proshlyakov, D. A.; Henshaw, T. F.; Monterosso, G. R.; Ryle, M. J.; Hausinger, R. P. *J. Am. Chem. Soc.* **2004**, *126*, 1022–1023. (b) Grzyska, P. K.; Appelman, E. H.; Hausinger, R. P.; Proshlyakov, D. A. *Proc. Natl. Acad. Sci. U.S.A.* **2010**, doi:10.1073/pnas.0911565107.
(16) Riggs-Gelasco, P. J.; Price, J. C.; Guyer, R. B.; Brehm, J. H.; Barr, E. W.; Bollinger, J. M., Jr.; Krebs, C. *J. Am. Chem. Soc.* **2004**, *126*, 8108–8109.
(17) Sinnecker, S.; Svensen, N.; Barr, E. W.; Ye, S.; Bollinger, J. M., Jr.; Neese, F.; Krebs, C. *J. Am. Chem. Soc.* **2007**, *129*, 6168–6179.
(18) (a) Hoffart, L. M.; Barr, E. W.; Guyer, R. B.; Bollinger, J. M., Jr.; Krebs, C. *Proc. Natl. Acad. Sci. U.S.A.* **2006**, *103*, 14738–14743. (b) Eser, B. E.; Barr, E. W.; Frantom, P. A.; Saleh, L.; Bollinger, J. M., Jr.; Krebs, C.; Fitzpatrick, P. F. *J. Am. Chem. Soc.* **2007**, *129*, 11334–11335. (c) Galonić, D. P.; Barr, E. W.; Walsh, C. T.; Bollinger, J. M., Jr.; Krebs, C. *Nat. Chem. Biol.* **2007**, *3*, 113–116. (d) Galonić, D. P.; Barr, E. W.; Matthews, M. L.; Koch, G. M.; Yonce, J. R.; Walsh, C. T.; Bollinger, J. M., Jr.; Krebs, C.; Riggs-Gelasco, P. J. *J. Am. Chem. Soc.* **2007**, *129*, 13408–13409. (e) Matthews, M. L.; Krest, C. M.; Barr, E. W.; Vaillancourt, F. H.; Walsh, C. T.; Green, M. T.; Krebs, C.; Bollinger, J. M., Jr. *Biochemistry* **2009**, 4331–4343.

II, either do not accumulate or only accumulate to levels that do not permit their spectroscopic characterization. However, models for **I** have been generated by using NO, which has one less valence electron than O_2, as an analogue for O_2. It has been demonstrated for several mononuclear nonheme iron enzymes, including an αKG-dependent dioxygenase, that the iron(II) site of the enzyme reacts with NO to yield a $\{FeNO\}^7$ species in the notation introduced by Enemark and Feltham,[20] which has an $S = 3/2$ electronic ground state.[21] Spectroscopic and computational studies indicate that the quartet ground state is best rationalized as a high-spin Fe(III) ($S_{Fe} = 5/2$) antiferromagnetically coupled to NO^- ($S_{NO} = 1$).[22] Although these NO-adducts may be good structural models for **I**, their electronic structure is very different from **I**, because they have one less valence electron than **I**, which is a $\{FeO_2\}^8$ species. We have therefore studied the NO-adduct of TauD:Fe(II):αKG:taurine complex, an $\{FeNO\}^7$ species that is termed TauD−$\{FeNO\}^7$ in the following, and its one-electron reduced form, TauD−$\{FeNO\}^8$. The latter species was generated by low-temperature (77 K) γ-radiolysis using a ^{60}Co source. This technique, also known as cryoreduction, offers the advantage of reducing metal clusters without structural changes. In this work, we have studied the TauD−$\{FeNO\}^{7,8}$ complexes experimentally and use the results to calibrate computational methods for their description.

Experimental Procedures

Protein Expression and Purification. TauD was prepared as previously described.[11]

Preparation of the {FeNO}^{7} Complex. On a Schlenck line, an anaerobic solution of the TauD:Fe(II):αKG:taurine complex (concentrations are 2.2 mM TauD, 1.54 mM ^{57}Fe(II), 5 mM αKG, and 5 mM taurine) was exposed to NO gas (∼1−1.5 atm) for ∼7 min at ambient temperature, subsequently transferred to an MBraun anaerobic chamber, transferred into Mössbauer or EPR sample holders, and subsequently anaerobically frozen in liquid nitrogen.

Cryoreduction of the {FeNO}^{7} Complex by Low-Temperature γ-Radiolysis. Frozen samples suitable for Mössbauer spectroscopy were irradiated in the γ-irradiation facility of the Breazeale nuclear reactor at the Pennsylvania State University using a ^{60}Co-source (activity 26 krad/h). A total dose of ca. 4.4 Mrad was delivered. During the γ-irradiation, the sample was kept in liquid nitrogen ($T = 77$ K).

Mössbauer and EPR Spectroscopy. The EPR and Mössbauer spectrometers have been described.[11] The Mössbauer isomer shifts quoted are relative to the centroid of the spectrum of a metallic foil of α-Fe at room temperature. Simulations of Mössbauer spectra were carried out with the program WMOSS (Web Research, Edina, MN). Some of the simulations are based on the commonly used spin Hamiltonian (eq 1),[23] in which the first three terms describe the electron Zeeman effect and ZFS of the total electron spin ground state, the fourth term represents the interaction between the electric field gradient and the nuclear quadrupole moment, the fifth term describes the magnetic hyperfine interactions of the electronic spin with the ^{57}Fe nucleus, and the last term represents the nuclear Zeeman interaction. The simulations were carried out with the assumption that the fluctuation rate of the electron spin is slow as compared to the ^{57}Fe nuclear Larmor frequency.

$$\mathbf{H} = \beta \mathbf{S}\cdot\mathbf{g}\cdot\mathbf{B} + D\left(\mathbf{S}_z^2 - \frac{S(S+1)}{3}\right) + E(\mathbf{S}_x^2 - \mathbf{S}_y^2) + \frac{eQV_{zz}}{12}[3\mathbf{I}_z^2 - I(I+1) + \eta(\mathbf{I}_x^2 - \mathbf{I}_y^2)] + \mathbf{S}\cdot\mathbf{A}\cdot\mathbf{I} - g_n\beta_n\mathbf{B}\cdot\mathbf{I} \quad (1)$$

Computational Details

Geometry Optimizations. The$\{FeNO\}^7$ and $\{FeNO\}^8$ complexes of TauD were modeled in this work by an Fe−NO core coordinated by two imidazole ligands (His) and one acetate ligand (Asp) forming a facial plane, and one α-ketopropionate (mimicking the cosubstrate α-KG) occupying the equatorial plane. Rigid surface scans and complete geometry optimizations were carried out with the B3LYP density functional[24] in the gas phase. The TZVP[25] (Fe, O, and N) and SV(P)[26] basis sets (other elements) were applied, in combination with the auxiliary basis sets TZV/J (Fe, O, and N) and SV/J (the remaining atoms).[27] All basis functions were taken from the Turbomole basis set library.[28] The RIJONX[29] approximation was used to accelerate the calculations. Because several broken symmetry solutions to the spin-unrestricted Kohn−Sham equations may be obtained for many of the species in this work, a general notation BS(m,n)[30] has been adopted. The nature of the solution is investigated by the corresponding orbital transformation,[30] which, via the corresponding orbital overlaps, demonstrates whether the system is to be described as a spin-coupled or a normal "pure" spin solution.[30]

Spectroscopic Parameters. Spectroscopic properties were obtained from additional single-point energy calculations at the optimized geometries. For this purpose, the B3LYP hybrid density functional was applied in combination with the CP(PPP) basis set for Fe,[31] and the TZVP[25] basis set for the nitrogen and oxygen atoms. The SV(P)[26] basis set was used for the remaining atoms.

Quadrupole splitting ΔE_Q values were obtained from electric field gradients V_i ($i = x, y, z$; V_i are the eigenvalues of the field gradient tensor) employing a nuclear quadrupole moment $Q(^{57}\text{Fe}) = 0.16$ barn:[32]

(19) Price, J. C.; Barr, E. W.; Hoffart, L. M.; Krebs, C.; Bollinger, J. M., Jr. *Biochemistry* **2005**, *44*, 8138–8147.

(20) Enemark, J. H.; Feltham, R. D. *Coord. Chem. Rev.* **1974**, *13*, 339–406.

(21) (a) Arciero, D. M.; Orville, A. M.; Lipscomb, J. D. *J. Biol. Chem.* **1985**, *260*, 14035–14044. (b) Chen, V. J.; Orville, A. M.; Harpel, M. R.; Frolik, C. A.; Surerus, K. K.; Münck, E.; Lipscomb, J. D. *J. Biol. Chem.* **1989**, *264*, 21677–21681. (c) Orville, A. M.; Lipscomb, J. D. *J. Biol. Chem.* **1993**, *268*, 8596–8607. (d) Rocklin, A. M.; Tierney, D. L.; Kofman, V.; Brunhuber, N. M. W.; Hoffman, B. M.; Christoffersen, R. E.; Reich, N. O.; Lipscomb, J. D.; Que, L., Jr. *Proc. Natl. Acad. Sci. U.S.A.* **1999**, *96*, 7905–7909. (e) Hegg, E. L.; Whiting, A. K.; Saari, R. E.; McCracken, J.; Hausinger, R. P.; Que, L., Jr. *Biochemistry* **1999**, *38*, 16714–16726. (f) Yang, T. C.; Wolfe, M. D.; Neibergall, M. B.; Mekmouche, Y.; Lipscomb, J. D.; Hoffman, B. M. *J. Am. Chem. Soc.* **2003**, *125*, 7056–7066.

(22) (a) Brown, C. A.; Pavlosky, M. A.; Westre, T. E.; Yan, Z.; Hedman, B.; Hodgson, K. O.; Solomon, E. I. *J. Am. Chem. Soc.* **1995**, *117*, 715–732. (b) Schenk, G.; Pau, M. Y. M.; Solomon, E. I. *J. Am. Chem. Soc.* **2004**, *126*, 505–515.

(23) Münck, E. In *Physical Methods in Bioinorganic Chemistry*; Que, L., Jr., Ed.; University Science Books: Sausalito, CA, 2000; pp 287−319.

(24) (a) Becke, A. D. *J. Chem. Phys.* **1993**, *98*, 5648–5652. (b) Lee, C. T.; Yang, W. T.; Parr, R. G. *Phys. Rev. B* **1988**, *37*, 785–789.

(25) Schäfer, A.; Huber, C.; Ahlrichs, R. *J. Chem. Phys.* **1994**, *100*, 5829–5835.

(26) Schäfer, A.; Horn, H.; Ahlrichs, R. *J. Chem. Phys.* **1992**, *97*, 2571–2577.

(27) (a) Eichkorn, K.; Treutler, O.; Ohm, H.; Häser, M.; Ahlrichs, R. *Chem. Phys. Lett.* **1995**, *242*, 652–660. (b) Eichkorn, K.; Weigend, F.; Treutler, O.; Ahlrichs, R. *Theor. Chem. Acc.* **1997**, *97*, 119–124.

(28) Ahlrichs, R.; et al. *Turbomole (5.3)*; Quantum Chemistry Group, University of Karlsruhe: Karlsruhe, Germany, 2000. The basis set can be downloaded from the ftp server of the Turbomole home page: http://www.turbomole.com.

(29) Neese, F.; Olbrich, G. *Chem. Phys. Lett.* **2002**, *362*, 170–178.

(30) (a) Kirchner, B.; Wennmohs, F.; Ye, S.; Neese, F. *Curr. Opin. Chem. Biol.* **2007**, *11*, 134–141. (b) Bart, S. C.; Chłopek, K.; Bill, E.; Bouwkamp, M. W.; Lobkovsky, E.; Neese, F.; Wieghardt, K.; Chirik, P. J. *J. Am. Chem. Soc.* **2006**, *128*, 13901–13912.

$$\Delta E_Q = \frac{1}{2} eQ \cdot V_z \cdot \sqrt{1 + \frac{1}{3}\eta^2} \quad (2)$$

Here, $\eta = (V_x - V_y)/V_z$ is the asymmetry parameter. Isomer shifts δ were calculated from the electron densities at the Fe nuclei ρ_0 employing the linear regression:

$$\delta = \alpha \cdot (\rho_0 - C) + \beta \quad (3)$$

Here, C is a constant of 11 800 au^{-3}, and $\alpha = -0.367$ au^3·mm/s and $\beta = +6.55$ mm/s are the fit parameters from our previous work.[32]

The magnetic hyperfine coupling tensor, **A**, of the ^{57}Fe center was calculated by taking the isotropic Fermi contact term, the first-order traceless dipolar contribution, and the second-order nontraceless spin−orbit contribution into account. The Fermi contact contributions for high-spin ferric species were scaled by a factor of 1.81 according to our earlier study.[32] Spin−orbit contributions to the hyperfine tensors were calculated as second-order properties employing the coupled perturbed (CP) Kohn−Sham theory.[33] The iron magnetic hyperfine coupling constants of the "genuine" antiferromagnetic state A_i^{AF} were calculated from the magnetic hyperfine coupling constants of the corresponding broken symmetry state A_i^{BS} by conversion into "site values" and multiplication by the spin projection coefficients C_i:[34]

$$A_i^{AF} = C_i \frac{A_i^{BS} M_s^{BS}}{\pm S_i} \quad (4)$$

The contributions of spin orbit coupling (SOC) to ZFS[35] were calculated by recently developed linear response theory[36] employing the hybrid B3LYP density functional. Here, the SOC contribution to the ZFS tensor is written as:

$$D_{kl}^{(SOC;M)} = f_M(S)\langle\langle h_k^{SOC}; h_l^{SOC}\rangle\rangle \quad (5)$$

In eq 5, $M = 0, \pm 1$ denotes contributions to the SOC term from excited states with $S' = S \pm 1$ ($S > 1/2$ is the total spin quantum number of the electronic state for which the ZFS tensor is computed), $f_M(S)$ is a spin-dependent prefactor ($f_0 = -(4S^2)^{-1}$; $f_{-1} = [2S(2S-1)]^{-1}$; $f_{+1} = [2(S+1)(2S+1)]^{-1}$), and $\langle\langle h_k^{SOC}; h_l^{SOC}\rangle\rangle$ is a shortcut notation for a spin−orbit linear response function. In a DFT framework, it is related to the derivatives of generalized spin-densities as explained in detail in ref 36.

The spin−spin coupling contributions to ZFSs are calculated from the equation of McWeeny and Mizuno:[37]

$$D_{kl}^{SS} = \frac{g_e^2}{4}\frac{\alpha^2}{S(2S-1)} \sum_{\mu\nu}\sum_{\kappa\tau} \{P_{\mu\nu}^{\alpha-\beta} P_{\kappa\tau}^{\alpha-\beta} - P_{\mu\kappa}^{\alpha-\beta} P_{\nu\tau}^{\alpha-\beta}\} \times \langle \mu\nu | r_{12}^{-5} \{3 r_{12,k} r_{12,l} - \delta_{kl} r_{12}\} | \kappa\tau \rangle \quad (6)$$

in which spin density matrix $\mathbf{P}^{\alpha-\beta}$ was obtained on the basis of the spin-unrestricted natural orbital (UNO) determinant.[38]

Total energy calculations were performed with the hybrid B3LYP density functional in combination with the new default basis sets of triple-ζ quality including high angular momentum polarization functions (def2-TZVPP)[39] for all elements. The density fitting (RIJONX) approximation has been employed for the coulomb term in B3LYP for which the def2-TZVPP/J auxiliary basis set[40] was used.

All calculations were performed with the ORCA program package.[41]

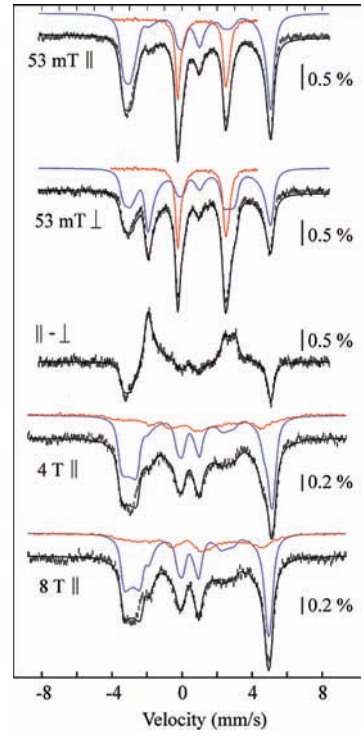

Figure 1. 4.2 K/variable-field Mössbauer spectra of a sample of TauD:Fe(II):αKG:taurine reacted with NO for 7 min at ambient temperature. The strength of the magnetic field and its orientation relative to the γ-beam is indicated in the spectra. The red lines are spectra of the reactant TauD:Fe(II):αKG:taurine complex, scaled to 27% of total intensity. The blue lines are simulations of TauD−{FeNO}^{7} (73% of total intensity) using the spin Hamiltonian parameters given in Table 1. The black lines represent the added contributions of the two components.

Results and Discussion

EPR and Mössbauer Spectroscopic Characterization of TauD−{FeNO}^{7}. The EPR spectrum of a sample of the TauD:Fe(II):αKG:taurine complex that was exposed to NO for 7 min at ambient temperature to form the {FeNO}^{7} species, termed TauD−{FeNO}^{7}, is shown in Figure S1. It exhibits a signal typical of an $S = 3/2$ species with effective g-values of ∼4, ∼4, and ∼2. From these values, we conclude that the rhombicity, E/D, is ∼0. It is essentially identical to the spectrum of TauD−{FeNO}^{7} reported by McCracken and co-workers[42] and similar to those of many other {FeNO}^{7} species of mononuclear nonheme enzymes and models thereof.[21]

The 4.2 K/variable-field Mössbauer spectra of a sample of TauD:Fe(II):αKG:taurine exposed to NO provide further insight into the electronic structure of TauD−{FeNO}^{7} (Figure 1). Analysis of the spectra reveals that the sample contains ∼27%

(31) Neese, F. *Inorg. Chim. Acta* **2002**, *337*, 181–192.
(32) Sinnecker, S.; Slep, L. D.; Bill, E.; Neese, F. *Inorg. Chem.* **2005**, *44*, 2245–2254.
(33) Neese, F. *J. Chem. Phys.* **2003**, *118*, 3939–3948.
(34) Sinnecker, S.; Neese, F.; Noodleman, L.; Lubitz, W. *J. Am. Chem. Soc.* **2004**, *126*, 2613–2622.
(35) Bencini, A.; Gatteschi, D. *EPR of Exchange Coupled Systems*; Springer-Verlag: Berlin, 1990.
(36) Neese, F. *J. Chem. Phys.* **2007**, *127*, 164112–164122.
(37) McWeeny, R.; Mizuno, Y. *Proc. R. Soc. London* **1961**, *259*, 554–577.
(38) Sinnecker, S.; Neese, F. *J. Phys. Chem. A* **2006**, *110*, 12267–12275.
(39) Weigend, F.; Häser, M.; Patzelt, H.; Ahlrichs, R. *Chem. Phys. Lett.* **1998**, *294*, 143–152.
(40) Weigend, F.; Köhn, A.; Hättig, J. *J. Chem. Phys.* **2002**, *116*, 3175–3183.
(41) Neese, F. *ORCA - an ab initio, Density Functional and Semiempirical Program Package*, 2.6.2008 ed.; Universität Bonn: Bonn, Germany, 2008.
(42) Muthukumaran, R. B.; Grzyska, P. K.; Hausinger, R. P.; McCracken, J. *Biochemistry* **2007**, *46*, 5951–5955.

Table 1. Comparison of Calculated and Experimental Geometric and Spectroscopic Parameters of TauD−{FeNO}^{7}

	exp.	^{4}**A**	^{4}**B**
ΔE (kcal/mol)		0	0.4
Fe−N (Å)	1.785[d]	1.877	1.879
N−O (Å)	1.163[d]	1.168	1.167
Fe−O_{C1OO} (αKG) (Å)	2.012[d]	2.055	2.057
Fe−$O_{C2=O}$ (αKG) (Å)	2.268[d]	2.370	2.381
Fe−N−O (deg)	146.0[d]	144.0	143.5
O−N−Fe−O_α (deg)	330.0[d]	336.9	162.2
D (cm^{-1})[a]	11.8	7.4	7.4 (*10.4*)[e]
E/D[a]	0.02	0.08	0.10 (*0.05*)[e]
δ (mm/s)	0.69	0.72	0.72 (*0.72*)[e]
ΔE_Q (mm/s)	−1.70	−1.55	−1.51 (*−1.74*)[e]
η	0.8	1.1	1.0 (*1.0*)
α, β, γ (deg)[b]	0, 0, 0	55, 153, −87	62, 165, −79 (*78, 178, −55*)[e]
A (MHz)[a]	−33.5, −34.1, −43.4	−39.3, −45.6, −49.7	−38.1, −43.7, −48.0 (*−30.4, −35.5, −47.5*)[e]
α, β, γ (deg)[c]	0, 0, 0	−53, 25, 82	78, 11, 21 (*58, 7, 18*)[e]

[a] Given with respect to the total spin, $S_{total} = 3/2$. [b] Euler angles rotating the electric field gradient tensor into the coordinate frame of the ZFS tensor. [c] Euler angles rotating the **A** tensor of ^{57}Fe into the coordinate frame of the ZFS tensor. [d] Taken from ref 44. [e] Italicized parameters were used for the simulations of TauD−{FeNO}^{7} shown in Figure S2.

of the starting TauD:Fe(II):αKG:taurine complex (blue lines) and ∼73% of TauD−{FeNO}^{7} (red lines). Prolonged reaction of the TauD:Fe(II):αKG:taurine complex with NO does not increase the yield of TauD−{FeNO}^{7}. Rather, formation of a high-spin Fe(III) species, which is identified by its diagnostic EPR feature at $g_{eff} \approx 4.3$ and its broad, magnetically split features in the 4.2 K/53 mT Mössbauer spectra (data not shown), is observed. Because the TauD:Fe(II):αKG:taurine complex is not reduced by γ-radiolysis at 77 K,[11] it does not interfere with the cryoreduction of TauD−{FeNO}^{7}. By contrast, the high-spin Fe(III) species generated after prolonged times with NO is expected to be cryoreduced to a Fe(II) complex, which would make the analysis of the Mössbauer spectra more complex. The spectral features of TauD−{FeNO}^{7} can be simulated with spin Hamiltonian parameters similar to those reported for other {FeNO}^{7} complexes with $S = 3/2$ ground state[43] and corroborate the view that TauD−{FeNO}^{7} contains a high-spin Fe(III) site.

Geometric Structure of TauD−{FeNO}^{7}. The models of TauD−{FeNO}^{7} with $S = 3/2$ ground states were generated by truncation of the second coordination sphere from the crystal structure of the NO-adduct of the related Fe(II)- and αKG-dependent enzyme clavaminate synthase.[44] Geometry optimizations were performed under the assumption of several possible spin-coupling schemes. The first of three possibilities represents "antiferromagnetic coupling" between a high-spin Fe(III) ($S_{Fe} = 5/2$) and an NO^- ($S_{NO} = 1$) as proposed by Solomon and co-workers in their model studies.[22] Such a state is represented by seven effectively unpaired electrons with five spin-up electrons occupying iron 3d-based orbitals and two spin-down electrons residing in NO-π* orbitals. Such a determinant has a well-defined $M_S = 3/2$ but is not a "pure" spin state, for example, $\langle \mathbf{S}^2 \rangle \neq S(S+1)$. The electron density and the potential energy surface from this broken symmetry (BS) calculation is expected to closely mimic a genuine $S = 3/2$ state with the same leading resonance structure, while the spin densities obtained from such an approach are unphysical. Deduction of the relevant spectroscopic parameters requires spin projection techniques. This calculation will be referred to as a BS(5,2) solution. The second possibility is a BS(4,1) calculation, which describes antiferromagnetic coupling between a high-spin ferrous ion ($S_{Fe} = 2$) and an NO$^\bullet$ radical ($S_{NO} = 1/2$). The third possibility is the direct calculation of a $M_S = 3/2$ Kohn−Sham determinant [formally equal to BS(3,0)], which could perhaps be interpreted as an intermediate-spin ferric ion ($S_{Fe} = 3/2$) bound to an NO^- ligand with $S_{NO} = 0$ or an Fe(I) oxidation state ($S_{Fe} = 3/2$) with a cationic NO^+ ligand ($S_{NO} = 0$).

The actual interpretation of the dominant resonance structure must then arise from a detailed inspection of the orbitals occupied in the Kohn−Sham solution. The various possibilities can, in principle, be distinguished by their relative energies as well as by comparing the predicted spectroscopic properties to the experimental data obtained for TauD−{FeNO}^{7}.

In converging the various broken-symmetry calculations, it was found that all calculations converged to the same BS(5,2) solution irrespective of which initial guess was employed. This solution can therefore be assigned with confidence to the lowest energy solution. Reasonable agreement between the fully optimized structure of TauD−{FeNO}^{7} (denoted hereafter as ^{4}**A**; in general, we denote model structures by bold-faced capital letters; the superscripted number indicates the spin multiplicity of that structure) and the experimentally determined structure[44] was achieved (Table 1); in particular, the N−O bond length and the Fe−N−O angle are well reproduced. As expected, the other weak metal ligand bond length shows larger deviations, but is still reasonable considering the relative low resolution (1.6 Å) of the protein X-ray crystallography[44] and the systematic error of the DFT method for such bond distances.[45]

Starting from the optimized geometry of ^{4}**A**, a rigidly scanned potential energy surface (PES, B3LYP/TZVP level) calculation has been performed to study the influence of the rotation of the bent NO ligand over the equatorial plane in TauD−{FeNO}^{7}. In contrast to the results obtained for the well-characterized doublet [(cyclam-ac)Fe(NO)]$^+$complex (cyclam-ac = 1,4,8,11-tetraazacyclotetradecane-1-acetic acid),[46] the PES for TauD−{FeNO}^{7} displays two well-defined minima (Figure 2). One minimum corresponds to the conformer ^{4}**A** where the NO group is situated above the carbonyl group of the αKG cosubstrate

(43) (a) Orville, A. M.; Chen, V. J.; Kriauciunas, A.; Harpel, M. R.; Fox, B. G.; Münck, E.; Lipscomb, J. D. *Biochemistry* **1992**, *31*, 4602–4612. (b) Hauser, C.; Glaser, T.; Bill, E.; Weyhermüller, T.; Wieghardt, K. *J. Am. Chem. Soc.* **2000**, *122*, 4352–4365.

(44) Zhang, Z.; Ren, J.-S.; Harlos, K.; McKinnon, C. H.; Clifton, I. J.; Schofield, C. J. *FEBS Lett.* **2002**, *517*, 7–12.

(45) (a) Neese, F. *J. Biol. Inorg. Chem.* **2006**, *11*, 702–711. (b) Neese, F. *Coord. Chem. Rev.* **2009**, *253*, 526–563.

(46) García Serres, R.; Grapperhaus, C. A.; Bothe, E.; Bill, E.; Weyhermüller, T.; Neese, F.; Wieghardt, K. *J. Am. Chem. Soc.* **2004**, *126*, 5138–5153.

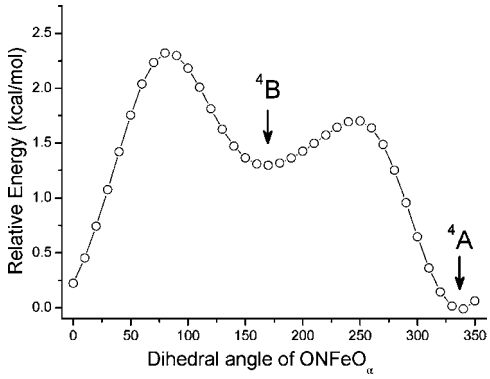

Figure 2. Rigidly scanned potential energy surface for the rotation of the NO group in TauD−{FeNO}^{7} (B3LYP/TZVP).

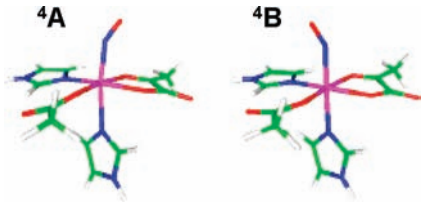

Figure 3. The optimized geometries of ^{4}**A** and ^{4}**B** as models for TauD−{FeNO}^{7}.

(thus serving as O_2 surrogate). In the other minimum (^{4}**B**), the NO ligand is located above the acetate ligand, representing the protein carboxylate ligand (Figure 3). In these two isomers, the NO ligand bends toward the π-acceptor groups (C═O), as predicted for metal nitrosyl complexes.[47] The bending mode distortion serves to minimize the σ-antibonding character of the NO lone pairs and the metal d_{xz} orbital and at the same time to maximize the d_{xz}-π^*_{ip} σ-bonding interaction.

Following complete geometry optimization, it turned out that ^{4}**B** is nearly isoenergetic with ^{4}**A** with very similar geometric features except for the relative orientation of NO with respect to αKG (Table 1). However, only the conformer ^{4}**A** is detected in the crystal structure of the {FeNO}^{7} species of clavaminate synthase. Because the two conformers are only separated by a barrier of ∼1.3 kcal/mol, it is conceivable that the protein destabilizes conformer ^{4}**B** by a few kcal/mol, such that it is not observed in the X-ray structure.

Electronic Structure of TauD−{FeNO}^{7}. To allow for the interpretation of the obtained Kahn−Sham solution in terms of more familiar chemical concepts, it is convenient to transform the canonical Kohn−Sham orbitals to corresponding MOs. A schematic MO diagram for the model ^{4}**A** is depicted in Figure 4. Analogous results are found for ^{4}**B** (not shown). One can easily identify five singly occupied spin-up MOs that are mainly localized on the iron center. In the spin-down manifold, two unpaired electrons reside in NO-π^* orbitals. Two iron-based MOs (d_{xz} and d_{yz}) have large spatial overlaps (S = 0.6−0.8) with NO-π^* based MOs in the spin-down set. The large overlaps indicate partial formation of a covalent bond between the high-spin Fe(III) and the triplet NO^- ligand. Thus, the results of these calculations are in full agreement with the studies of Brown et al.,[22] who have suggested this electronic structure pattern for {FeNO}^{7} complexes with an S = 3/2 ground state. The corresponding orbital transformation represents a convenient

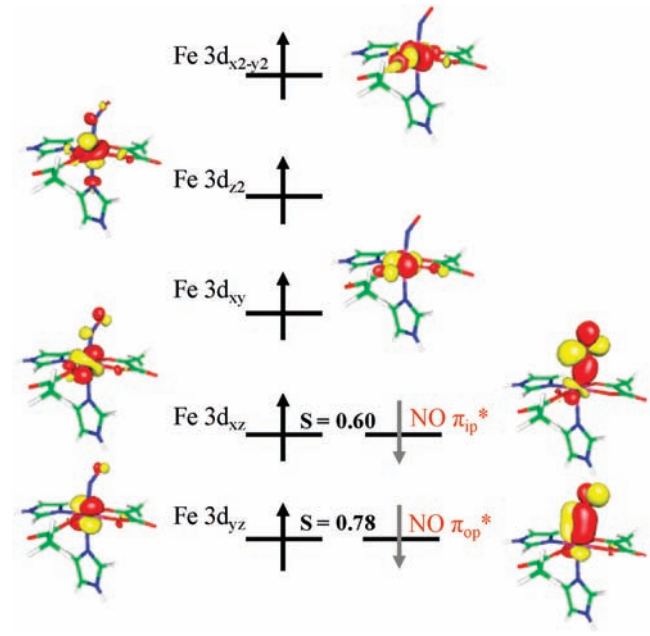

Figure 4. Schematic MO diagram for ^{4}**A**. The spin-coupled pairs are represented by corresponding orbitals, whereas for the remaining orbitals quasi-restricted orbitals are employed.

display of this bonding situation, which may not be straightforward to identify in terms of delocalized canonical MOs. As expected and seen in Figure 4, both σ- and π-interactions are present in the upper valence region: d_{xz} has a pseudo-σ-bonding interaction with NO π^*_{ip} and d_{yz} a π-bonding interaction with NO π^*_{op}. The remaining three singly occupied MOs are essentially nonbonding (d_{xy}) and σ-antibonding (d_{x2-y2} and d_{z2}) orbitals. The large metal contribution (∼15%) in the NO π^*-orbitals may be viewed as charge donation of NO to the metal center. This backbonding process removes the electron density from the NO-π^* orbitals and hence strengthens the N−O bond relative to free NO^-. Likewise, the back-bonding shows up as appreciable NO-π^* character (∼5%) in the metal-based MOs.

The Mössbauer isomer shift (δ), the quadrupole splitting (ΔE_Q), the asymmetry parameter (η), Fe hyperfine tensor (**A**), axial ZFS parameter (D), and the rhombicity parameter (E/D) were calculated for ^{4}**A** and ^{4}**B** and are reported in Table 1. The calculated parameters agree well with those experimentally observed for TauD−{FeNO}^{7} and other {FeNO}^{7} species,[43] thus lending further support of the electronic structure description advocated above. However, the quality of the simulations using the exact values of the calculated parameters for ^{4}**A** and ^{4}**B** is not entirely satisfactory. This behavior can be rationalized by the fact that the simulations strongly depend on the magnitude and relative orientation of the ZFS tensor, the ^{57}Fe hyperfine tensor, and the electric field gradient tensor at the ^{57}Fe nucleus, all of which are highly anisotropic. Therefore, even small variations of a single parameter within a few percent of its value may alter the simulated spectrum dramatically. Using the calculated parameters of ^{4}**B** as a starting point, it is possible to obtain good simulations by selectively adjusting some of the parameters. In Figure S2, we show simulations generated by using the italicized parameters of Table 1. The most significant deviations are the magnitude of the axial ZFS parameter, D, which is found to be approximately twice as large as calculated, and the absolute magnitude of A_x and A_y, both of which are ∼20% smaller. Although large deviations in D are typical, the deviation of the anisotropy of the hyperfine tensor is somewhat

(47) Hoffmann, R.; Chen, M. M. L.; Elian, M.; Rossi, A. R.; Mingos, D. M. P. *Inorg. Chem.* **1974**, *13*, 2666–2675.

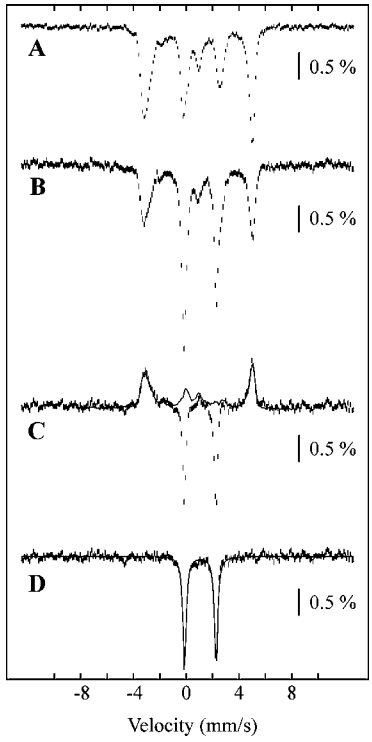

Figure 5. 4.2 K/53 mT Mössbauer spectra of a sample of TauD:Fe(II):αKG:taurine reacted with NO before (A) and after (B) cryoreduction. The difference spectrum (C, hashed marks) reveals that TauD−{FeNO}^{7} (solid line, 31% of total intensity) is converted to a quadrupole doublet during cryoreduction. Removal of the contribution of TauD−{FeNO}^{7} yields the hashed-marked spectrum (D), which can be simulated with a quadrupole doublet (solid line) with parameters quoted in the text.

greater than usual.[32] Nevertheless, the calculated spin Hamiltonian parameter set as a whole reproduces the experimentally observed features well. The predicted spectroscopic parameters for the conformer ^{4}**A** are similar to those for ^{4}**B**, in agreement with the very similar electronic structures of the FeNO core for both conformers.

Mössbauer-Spectroscopic Characterization of TauD−{FeNO}^{8}. The 4.2 K/53 mT Mössbauer spectra of a sample of TauD:Fe(II):αKG:taurine reacted with NO recorded before and after cryoreduction are shown in Figure 5A and B, respectively. The effect of cryoreduction is best seen in the difference spectrum (Figure 5C), which clearly reveals that a fraction of TauD−{FeNO}^{7} (solid line pointing upward, 31% of the total intensity) is converted to a novel species, which exhibits a quadrupole doublet under these experimental conditions, as is expected for the one-electron reduced form of TauD−{FeNO}^{7}. Accordingly, this species is termed TauD−{FeNO}^{8}. Adding back the contribution of TauD−{FeNO}^{7} to the difference spectrum yields the reference spectrum of TauD−{FeNO}^{8} (Figure 5D). The latter can be simulated with a sharp (Γ = 0.30 mm/s) quadrupole doublet (31% intensity) with the following parameters: $\delta = 1.07$ mm/s and $|\Delta E_Q| = 2.39$ mm/s.

The isomer shift increases from 0.71 mm/s in TauD−{FeNO}^{7} to 1.07 mm/s in TauD−{FeNO}^{8}. This increase by 0.36 mm/s suggests that the high-spin Fe(III) center of the {FeNO}^{7} species is reduced to formally a high-spin Fe(II) site with $S_{Fe} = 2$ and, consequently, that the NO-ligand remains as an NO$^-$. Because the NO$^-$ ligand will have either a diamagnetic ($S_{NO} = 0$) or paramagnetic ($S_{NO} = 1$) ground state, different total spin states of $S = 1$, 2, or 3 are conceivable as ground states for TauD−{FeNO}^{8}.

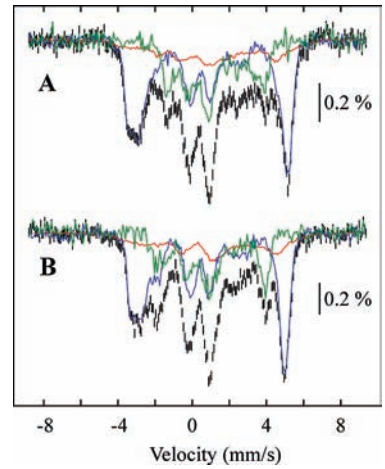

Figure 6. 4.2 K Mössbauer spectra of a cryoreduced sample of the NO-reacted TauD:Fe(II):αKG:taurine complex recorded in externally applied magnetic fields of 4 T (A) and 8 T (B). The contributions of experimental reference spectra of TauD:Fe(II):αKG:taurine complex (20%), TauD−{FeNO}^{7} (49%), and TauD−{FeNO}^{8} (31%) are shown as solid lines in red, blue, and green, respectively.

To characterize TauD−{FeNO}^{8} in more detail, we collected Mössbauer spectra in externally applied magnetic fields of 4 and 8 T (Figure 6). From the analysis of these spectra, as well as the 4.2 K/53 mT spectrum (Figure 5B), we conclude that the cryoreduced sample contains 20% of reactant TauD:Fe(II):αKG:taurine complex, 49% of TauD−{FeNO}^{7}, and 31% of TauD−{FeNO}^{8}. Removal of the features of the former two components from the raw data yields the reference spectra of TauD−{FeNO}^{8} (Figure 6, green lines).

In general, the analysis of magnetic Mössbauer spectra of high-spin Fe(II) compounds is challenging, not only because they depend on many parameters (i.e., the ZFS parameters D and E/D of the $S = 2$ ground state, the isomer shift δ, the quadrupole splitting parameter ΔE_Q, the asymmetry parameter η, the three components of the hyperfine tensor **A**, and two sets of Euler angles rotating the electric field gradient tensor and hyperfine tensor into the coordinate frame of the ZFS tensor), but also because the **A**-tensor and electric field gradient tensor exhibit significant anisotropy. Because of this complexity, many spectra recorded in different externally applied fields and at different temperatures are required to determine the many spectroscopic parameters of a high-spin Fe(II) center unambiguously, as was elegantly done by Münck and co-workers for the characterization of the nonheme Fe(II) center of protocatechuate-3,4-dioxygenase.[48] Characterization of TauD−{FeNO}^{8} is further complicated by the fact that its spin ground state is not known with certainty, and that the sample contains only 31% of it. Therefore, we have not explored the parameter space systematically. Rather, we have explored whether or not the spectroscopic parameters predicted computationally for hypothetical models of TauD−{FeNO}^{8} are compatible with the experimental data. This analysis is presented below.

Geometric Structure of TauD−{FeNO}^{8}. As explained above, the total spin state as well as the valence state of the central iron could not be unambiguously assigned from the experiments for TauD−{FeNO}^{8}. The main purpose of our calculations was to provide this information using the spectroscopically calibrated calculations described above. Therefore, geometries of

(48) Zimmerman, R.; Huynh, B. H.; Münck, E.; Lipscomb, J. D. *J. Chem. Phys.* **1978**, *69*, 5463–5467.

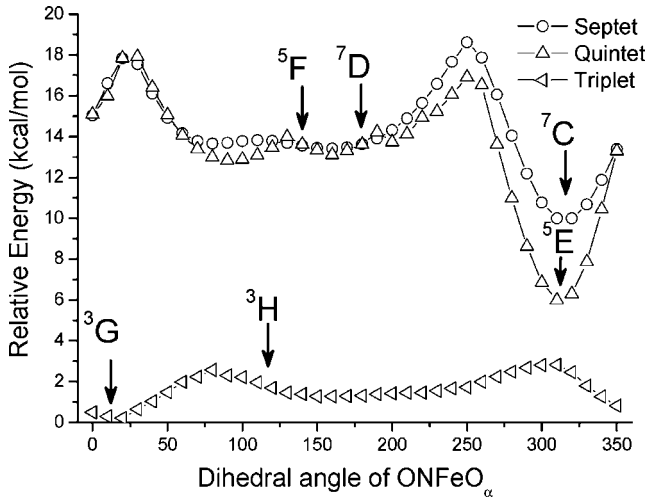

Figure 7. Rigid scanned potential energy surface for the rotation of the NO ligand in TauD−{FeNO}^{8}. The dihedral angles for the various model structures are indicated.

TauD−{FeNO}^{8} species were optimized on the septet, quintet, and triplet surface starting from the geometry of ^{4}**A**. For the triplet TauD−{FeNO}^{8} species, three different initial guesses were employed. The BS(2,0) state could represent an intermediate-spin ferrous center ($S_{Fe} = 1$) bound to an NO^- ligand with $S_{NO} = 0$ or a low-spin ferrous center ($S_{Fe} = 0$) coordinated to a high-spin NO^- ligand ($S_{NO} = 1$). The BS(3,1) state might best be described as consisting of an intermediate-spin ferric ion ($S_{Fe} = 3/2$) antiferromagnetically coupled to an NO^{2-} ($S_{NO} = 1/2$) radical ligand or a high-spin Fe(I) ion ($S_{Fe} = 3/2$) to an $NO^{\bullet}$ radical ($S_{NO} = 1/2$). Finally, a BS(4,2) solution may feature a high-spin ferrous ion ($S_{Fe} = 2$) antiferromagnetically coupled to an NO^- with $S_{NO} = 1$. Similar to the situation found in the case of TauD−{FeNO}^{7}, all calculations [BS(2,0), BS(3,1), and BS(4,2)] lead to the same solution that is best characterized as BS(4,2).

On the quintet surface, two solutions [BS(4,0) and BS(5,1)] were attempted. The BS(4,0) state represents a high-spin Fe(II) center ($S_{Fe} = 2$) coordinated to a diamagnetic NO^- ligand. BS(5,1) may best be interpreted as a high-spin ferric ion ($S_{Fe} = 5/2$) bound to an NO^{2-} ($S_{NO} = 1/2$) radical ligand. Both attempts converged to BS(5,1).

Finally, BS(6,0) stands for ferromagnetic coupling between a high-spin Fe(II) ($S_{Fe} = 2$) and an NO^- ligand ($S_{NO} = 1$) or a high-spin Fe(III) ($S_{Fe} = 5/2$) ion and an NO^{2-} ligand ($S_{NO} = 1/2$).

Before discussing the optimized structures, it is interesting to study the O−N−Fe−$O_{\alpha KG\text{-}keto}$ dihedral angle in TauD−{FeNO}^{8}, which describes the rotation of the bent NO ligand over the equatorial plane. A rigidly scanned PES (B3LYP/TZVP) starting from ^{7}**C**, ^{5}**E**, and ^{3}**G** for the different spin multiplicities is shown in Figure 7.

Following the rigid surface scanning, a complete geometry optimization was performed on each apparent minimum. The optimized geometries are shown in Figure 8. All PESs of TauD−{FeNO}^{8} feature a double minimum behavior; the two minima differ by the relative NO orientations with respect to αKG. Starting from each local minimum, two different structures for each spin multiplicity were found, resulting in a total of six different geometries (Figure 8) that are to be tested as candidates for the actual TauD−{FeNO}^{8} species in property calculations. We note that the orientation of the NO ligand for ^{7}**D**, ^{5}**F**, and ^{3}**H** does not correspond to the minimum of the PES. This behavior is presumably due to the fact that the minima corresponding to these structures are very shallow.

Furthermore, we considered the possibility that TauD−{FeNO}^{8} may be protonated to form a TauD−{FeHNO}^{8} species, because the transfer of the electron during cryoreduction may lead to transfer of a nearby proton to the active site for charge balance. To test this hypothesis, the corresponding protonated species for each TauD−{FeNO}^{8} model structure have also been interrogated computationally. The results are summarized in the Supporting Information. However, all protonated forms were found to best be described as high-spin ferric species. Consistently, their calculated Mössbauer parameters (in particular, the isomer shift) are clearly incompatible with the experimental data. Hence, all of these models are ruled out as candidates for the structure of TauD−{FeNO}^{8}.

Comparison of the geometries of TauD−{FeNO}^{8} complexes of varying spin multiplicities reveals that the triplet species exhibit the shortest Fe−N_{NO} bond distances and different NO orientation with respect to αKG as indicated by the O_{NO}−$C2_{\alpha KG}$ distance and O−N−Fe−O_α dihedral angles. The N−O bonds in all TauD−{FeNO}^{8} species are moderately longer (0.039−0.080 Å) than that in the parent TauD−{FeNO}^{7} species.

From an energetic point of view, only the triplet species appear to be viable candidates for the elusive paramagnetic TauD−{FeNO}^{8} species, because the quintet and septet models are disfavored by approximately 10 kcal/mol. This energy difference is considered to be larger than the methodological uncertainty.[49] The conclusion that TauD−{FeNO}^{8} is a triplet species is also corroborated by the comparison of the calculated and experimental spin Hamiltonian parameters for the six possible model structures (see below).

Electronic Structure of TauD−{FeNO}^{8}. Before discussing the calculated spectroscopic parameters, a description of the Fe−NO bonding in the three possible spin states is provided. This will help to understand why the quintet and septet states can be ruled out as candidates for TauD−{FeNO}^{8}.

i. Septet State. A qualitative MO scheme of the septet TauD−{FeNO}^{8} (^{7}**C**) is shown in Figure 9. Of the five metal-based d orbitals, four are singly occupied and one is doubly occupied. The remaining two unpaired electrons mainly reside in the NO-π^* orbitals, thus yielding an overall septet state. The electronic structure of this septet species may best be interpreted as consisting of a high-spin ferrous center ($S_{Fe} = 2$) ferromagnetically coupled to an NO^- ligand ($S_{NO} = 1$). However, some electron delocalization from the NO π_{ip}^* orbital to the αKG π^*-orbital can be identified. Thus, a partial bond is formed

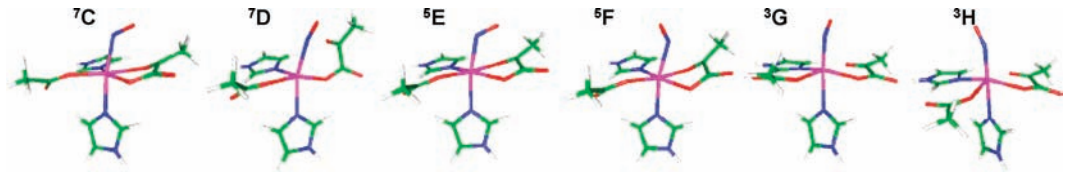

Figure 8. Geometries of TauD−{FeNO}^{8} models with different spin multiplicities.

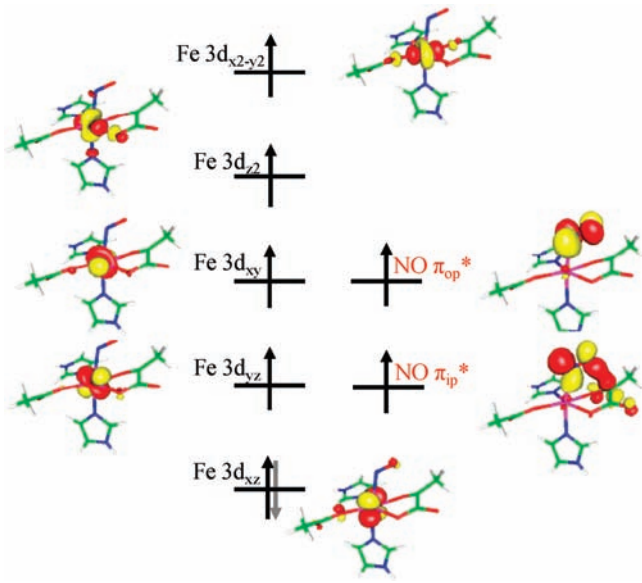

Figure 9. Schematic MO diagram for ^{7}**C**. Quasi-restricted orbitals are employed.

Table 2. Key Structural Features of TauD−{FeNO}^{8} with Different Spin Multiplicities and the Relative Energy Difference among Them

{FeNO}^{8}	^{7}**C**	^{7}**D**	^{5}**E**	^{5}**F**	^{3}**G**	^{3}**H**
ΔE (kcal/mol)	11.3	11.7	9.1	10.9	0.8	0
Fe−N (Å)	2.246	2.112	2.034	2.138	1.992	1.860
N−O (Å)	1.227	1.243	1.214	1.207	1.223	1.211
Fe−O_{C1OO} (αKG) (Å)	2.067	2.048	2.074	2.089	2.144	2.201
Fe−$O_{C2=O}$ (αKG) (Å)	2.403	4.057	2.356	2.359	2.495	2.501
O_{NO}−C2 (αKG) (Å)	2.582	3.639	2.495	3.686	3.671	4.664
Fe−N−O (deg)	122.7	148.8	124.0	127.0	130.5	154.2
O−N−Fe−O_α (deg)	315.1	221.8	312.5	187.1	21.8	94.3

between the distal oxygen atom of NO and C2 of αKG. Analogous results were obtained for ^{7}**D**, except that the partial bonding between NO and αKG is missing because there is no spatially favorable pathway for electron delocalization available. However, the calculated energies (Table 2) reveal that the partial O_{NO}−C2 bond must be extremely weak, because it only accounts for less than 1 kcal/mol stabilization energy.

ii. Quintet State. A BS(5,1) solution was found on the quintet surface irrespective of which initial guess was employed. As shown in Figure 10, one can identify one doubly occupied and four singly occupied orbitals that are of predominant Fe-3d character. In the spin-up manifold, the last SOMO is mainly based on the NO-π^*_{ip} orbital. In the spin-down manifold, one unpaired electron resides in the NO-π^*_{op} orbital, thus leading to an overall quintet state. Thus, the quintet TauD−{FeNO}^{8} species represents a high-spin ferrous ion ($S_{Fe} = 2$) coordinated to an NO^- in its first excited singlet state ($S_{NO} = 0$). By inspection of Figure 10, a spin-coupled pair consisting of the Fe-d_{z2} and the NO-π^*_{ip} fragment orbitals with a substantial mutual overlap is found via the corresponding orbital transformation. As expected, this situation leads to rather strong antiferromagnetic coupling. Therefore, the energy gained by the exchange coupling compensates for the loss in energy accompanied with the creation of the excited singlet state of the NO ligand. Hence, this situation is another example of "excited state" coordination that is driven by strong metal−ligand

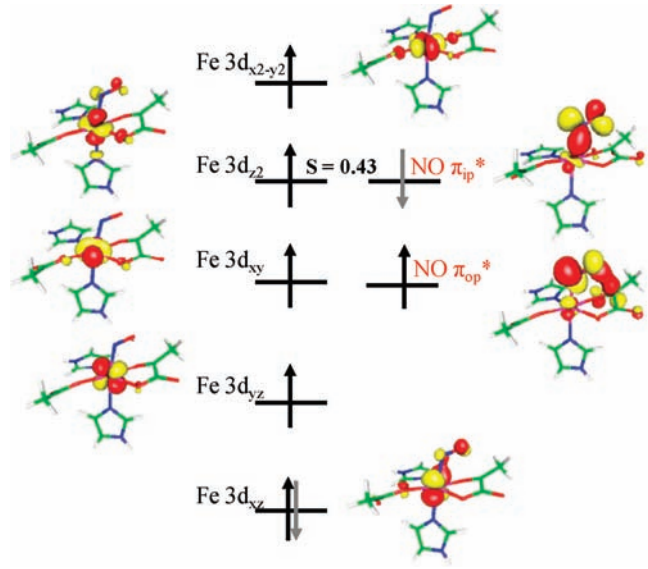

Figure 10. Schematic MO diagram for ^{5}**E**. The spin-coupled pair is represented by corresponding orbitals, whereas for the remaining orbitals quasi-restricted orbitals are employed.

exchange coupling.[50] Similar to the situation found for the septet species, a partial bond between the distal O atom and C2 of αKG is identified in ^{5}**E**, whereas it is missing in ^{5}**F**. The interaction in ^{5}**E** is stronger than that in ^{7}**C** as evidenced by the shorter O_{NO}−$C2_{\alpha KG}$ distance (Table 2). This may rationalize the fact that ^{5}**E** is stabilized by 1.8 kcal/mol relative to ^{5}**F**, while the corresponding energy separation between the two septet species is merely 0.4 kcal/mol.

iii. Triplet State. The molecular orbital diagrams computed for ^{3}**G** and ^{3}**H** are presented in Figures 11 and 12. The MOs of the triplet TauD−{FeNO}^{8} species closely resemble those of the septet state except that the two NO-π^* orbitals are occupied by two β-electrons. Thus, two spin-coupled pairs are formed. Because of the different Fe−N−O angle in ^{3}**G** and ^{3}**H**, the σ-pathway is composed of the Fe-d_{z2} and NO-π^*_{ip} orbitals in ^{3}**G** with a smaller Fe−N−O angle of 130°, while in ^{3}**H** it consists of the Fe-d_{xz} and NO-π^*_{ip} orbitals. By contrast, the π-pathway involves the same partners (the Fe-d_{yz} and NO-π^*_{op} orbitals) in the two triplet species. Thus, this electronic structure corresponds to a high-spin Fe(II) ($S_{Fe} = 2$) antiferromagnetically bound to an NO^- ligand with $S_{NO} = 1$. In fact, the electronic structure of ^{3}**H** closely resembles that of ^{4}**A** and ^{4}**B** because all of these states involve the same bonding partners for the two backbonding pathways. The only difference is that the essentially nonbonding Fe-d_{xy} orbital is doubly occupied in the former, while it is singly occupied in the latter. There are two backbonding pathways in the triplet species as evidenced by the shortest Fe−NO bond length among all spin multiplicities. This may rationalize the much lower energy of the triplet TauD−{FeNO}^{8} species relative to the quintet and septet species. Relative to the electronic structures of TauD−{FeNO}^{7}, the extra electron is accepted by the t_{2g} subshell (d_{xz} in ^{3}**G** and d_{xy} in ^{3}**H**). Therefore, one might expect that another triplet form may exist, in which the Fe-d_{yz} orbital is doubly occupied. However, no local minimum could be found for this electronic structure. If such a species existed, the π-backbonding would

(49) Siegbahn, P. E. M. *J. Biol. Inorg. Chem.* **2006**, *11*, 695–701.
(50) Ghosh, P.; Bill, E.; Weyhermüller, T.; Neese, F.; Wieghardt, K. *J. Am. Chem. Soc.* **2003**, *125*, 1293–1308.

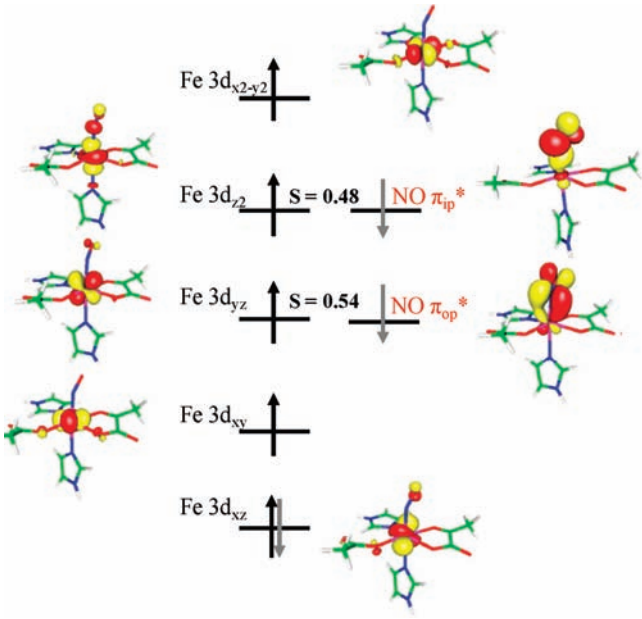

Figure 11. Schematic MO diagram for ^{3}**G**. The spin-coupled pairs are represented by corresponding orbitals, whereas for the remaining orbitals quasi-restrict orbitals are employed.

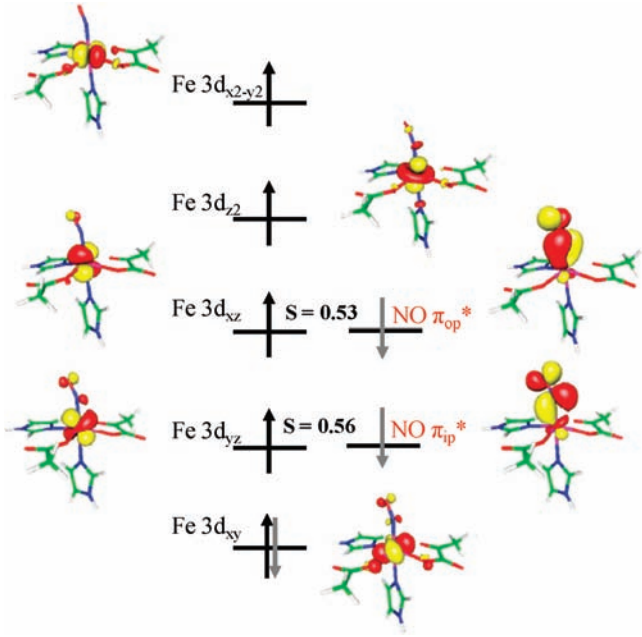

Figure 12. Schematic MO diagram for ^{3}**H**. The spin-coupled pair represents corresponding orbitals, whereas for the remaining orbitals quasi-restrict orbitals are employed.

be missing, because no other Fe 3d-based orbital but Fe-d$_{yz}$ has appropriate symmetry to interact with the NO-π^*_{op} orbital. However, there are two possible combinations for the σ-backbonding pathway, because both the Fe-d$_{xz}$ and the -d$_{z2}$ orbitals can interact with the NO-π^*_{ip} orbital as identified in ^{3}**H** (Fe-d$_{xz}$ + NO-π^*_{ip}) and ^{3}**G** (Fe-d$_{z2}$ + NO-π^*_{ip}).

A salient feature of the geometries of the triplet TauD−{FeNO}^{8} species is that the NO ligand is not situated above the π-acceptors (C═O) as observed for TauD−{FeNO}^{7}. This geometric feature may be rationalized by the fact that the 3d orbitals of the ferrous center are energetically closer to the NO-π^* orbitals than those of the ferric ion. In other words, TauD−{FeNO}^{8} features more pronounced backbonding between the iron center and the NO ligand. This is consistent with the shorter Fe−NO and longer N−O bond distances in ^{3}**H** as compared to those in ^{4}**A** and ^{4}**B**. Moreover, the π-accepting ability of the Fe-3d orbitals in TauD−{FeNO}^{8} may compete with or even exceed that of the C═O groups, thus leading to the observed geometric structure of the triplet TauD−{FeNO}^{8} species. However, the Fe-3d orbitals can act as electron acceptors only in the spin-down manifold. Therefore, the septet and quintet TauD−{FeNO}^{8} species have to employ the C═O groups as the electron acceptors in the spin-up manifold as identified by the partial bonding between the distal O atom of NO and the C2 atom of αKG in ^{7}**C** and ^{5}**E**.

Analysis of Magnetic Mössbauer Spectra of TauD−{FeNO}^{8} and Comparison to Computationally Predicted Mössbauer Parameters. The fact that the TauD−{FeNO}^{8} species gives rise to a quadrupole doublet in a small external magnetic field, but to magnetically split spectra in large external magnetic fields, is typical of a paramagnetic species with an integer spin ground state. The 4 and 8 T reference spectra cannot be analyzed with the assumption of a diamagnetic ($S = 0$) ground state (Figure S3), fully consistent with our hypothesis that TauD−{FeNO}^{8} has either an $S = 1$, 2, or 3 ground state. The additional splitting observed in the spectra is due to the internal magnetic field at the ^{57}Fe nucleus. The internal magnetic field is given by $\mathbf{B}_{int} = -\langle\mathbf{S}\rangle\cdot\mathbf{A}/g_N\beta_N$, in which $\langle\mathbf{S}\rangle$ represents the spin expectation value.[23] The latter is strongly dependent on the value of the spin S and the ZFS parameters D and E/D.

The calculated Mössbauer parameters for TauD−{FeNO}^{8} based on the optimized geometries are summarized in Table 3. The calculated isomer shifts for all six model structures closely match the experimental value and therefore do not allow us to discern among those structures. However, the calculated values of the quadrupole splitting parameter vary considerably. We consider structures ^{5}**F** and ^{3}**G** as unlikely candidates for TauD−{FeNO}^{8}, because the absolute value of ΔE_Q deviates by 1.04 and 0.89 mm/s from the experimental value, respectively. These deviations are greater than the typical uncertainty for this parameter (0.5 mm/s).[51] For the remaining four structures, the deviations of the calculated ΔE_Q values range from 0.34 mm/s for ^{3}**H** to 0.65 mm/s for ^{7}**D**. Thus, comparison of the calculated and experimental ΔE_Q values does not allow us to eliminate any of these structures as models for TauD−{FeNO}^{8}.

The septet structures are ruled out as possible candidates for TauD−{FeNO}^{8} for the following reason. To match the experimentally observed splitting, the internal magnetic field needs to be approximately 28 MHz (assuming that $\mathbf{B}_{int}$ is aligned antiparallel to the external field). Assuming that the ^{57}Fe hyperfine tensor is close to the Fermi contact term ($\mathbf{A}_{S=3} = (2/3)\cdot(-28)$ MHz, in which 2/3 is the appropriate spin coupling coefficient),[35] the spin expectation value $|\langle\mathbf{S}\rangle|$ needs to ∼1.5, which in turn requires that the ZFS parameter $|D|$ of the $S = 3$ spin state is approximately 20 cm^{-1}. Because $D_{S=3}$ is dominated by d_{Fe} [$D_{S=3} = (4/10)\cdot d_{Fe} + (1/15)\cdot d_{NO}$], this would require that $|d_{Fe}|$ is approximately 50 cm^{-1}. Although high-spin Fe(II) sites can have ZFS parameters of this magnitude,[52] this value is unusually large. As an alternative way to model the data, we

(51) Godbout, N.; Havlin, R.; Salzmann, R.; Debrunner, P. G.; Oldfield, E. *J. Phys. Chem. A* **1998**, *102*, 2342–2350.
(52) Boča, R. *Coord. Chem. Rev.* **2004**, *248*, 757–815.

Table 3. Calculated Spin Hamiltonian Parameters for Models of TauD−{FeNO}^{8}

parameter	^{7}**C**	^{7}**D**	^{5}**E**	^{5}**F**	^{3}**G**	^{3}**H**
S_{total}	3	3	2	2	1	1
D (cm^{-1})[a]	1.65	−1.8	−3.9 (*17.5*)[d]	−3.2	26.7	−12.6
E/D[a]	0.27	0.16	0.19	0.17	0.21	0.03 (*0.16*)[d]
δ (mm/s)	1.09	1.04	1.02	1.05	1.11	1.13
ΔE_Q (mm/s)	2.95	3.04	2.86	3.43	3.28	2.73
η	0.25	0.38	0.61	0.36	0.89	0.16
α, β, γ (deg)[b]	79.4, 78.1, −46.8	86.5, 81.8, 77.2	−86.2, 107.3, 71.8	11.6, 70.1, −72.9	−17.9, 134.0, 40.5	−69.2, 24.4, −15.0
A (MHz)[a]	1.1, −9.5, −12.0	−0.4, −10.7, −12.7	−8.7, −24.3, −26.5 (*−13.1, −24.3, −26.5*)[d]	−9.6, −25.0, −28.5	−14.5, −34.4, −48.8	−7.3, −29.2, −33.0
α, β, γ (deg)[c]	−89.7, 48.0, −59.3	43.1, 93.4, −31.5	−86.3, 107.3, 71.8	−17.9, 94.8, 48.5	−4.7, 23.4, 86.1	73.3, 65.4, −58.6

[a] Given with respect to the total spin, S_{total}. [b] Euler angles rotating the electric field gradient tensor into the coordinate frame of the ZFS tensor. [c] Euler angles rotating the **A** tensor of ^{57}Fe into the coordinate frame of the ZFS tensor. [d] Italicized parameters were used for the simulations of TauD−{FeNO}^{8} shown in Figure S4 and Figure 14.

have used the calculated spin Hamiltonian parameters to simulate the spectra. However, the position and intensities are inconsistent with these parameters. In addition, the total energy of ^{7}**C** and ^{7}**D** models is significantly higher than those of the triplet models, thus effectively ruling them out as models for TauD−{FeNO}^{8}.

Next, we evaluate the parameters of ^{5}**E**. Simulations using the parameters calculated for ^{5}**E** do not match the experimental data well (Figure S4, red lines). The overall splitting of the simulations is much greater than that experimentally observed. This is due to the negative sign of D, which produces a large $|\langle S_z\rangle|$ value for the ground state. Changing D from −3.9 to +17.5 cm^{-1} [i.e., change the sign of D and increase its magnitude by ∼4-fold] and changing **A** of ^{57}Fe from (−8.7, −24.3, −26.5) MHz to (−26.5, −24.3, −13.1) MHz [i.e., interchange A_x and A_z, and increase the absolute magnitude of the smallest component by ∼50%] yields acceptable results (Figure S4, blue lines). However, these changes, in particular those for D, are rather significant, although we realize that the predicted D-value is not accurate. Because of the previous argument and the fact that the total energy of ^{5}**E** is ∼9 kcal higher than those of the triplet states, we disfavor ^{5}**E** as a potential candidate for TauD−{FeNO}^{8}.

Finally, we evaluate the parameters calculated for ^{3}**H**. Simulations of the reference spectra of TauD−{FeNO}^{8} with the computed parameters are shown in Figure 13 as red lines. The simulation of the 8 T spectrum fits remarkably well, while the observed overall splitting in the 4 T spectrum is less than that of the simulation. Nevertheless, the general shape of the simulation is in our view surprisingly good. Changing the rhombicity, E/D, from 0.03 to 0.16 improves the quality of the simulation of the 4 T spectrum considerably, but does not affect the 8 T spectrum significantly (blue lines in Figure 14). The reason for this behavior is that the increase in E/D reduces the magnitude of $|\langle S_z\rangle|$, which is the dominant component of $|\langle \mathbf{S}\rangle|$ for $D < 0$, by ∼12% in an external 4 T field, whereas the value of $|\langle S_z\rangle|$ remains essentially constant for varying E/D in an 8 T field (calculated for $D = -12.6$ cm^{-1}). Of all calculated parameters, E/D is expected to be the one with the greatest uncertainty, because it is defined as $(D_{xx} - D_{yy})/D_{zz}$, and each of the three principal components of the ZFS tensor has significant calculated uncertainty. The E/D value arises from the very subtle differences in the smallest **D**-tensor components, rendering the calculated E/D values unreliable.[53] Thus, we conclude that the spin Hamiltonian parameters calculated for ^{3}**H** match the experimental data well and provide good evidence

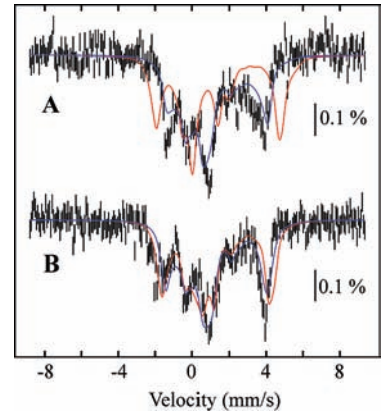

Figure 13. 4.2 K Mössbauer reference spectra of TauD−{FeNO}^{8} recorded in external fields of 4 T (A) and 8 T (B) (hashed marks) and spin Hamiltonian simulations thereof. The red lines are simulations using the parameters for ^{3}**H** given in Table 3, except for the values of δ and ΔE_Q for which we used the values determined using the parameters obtained from the 53 mT spectrum ($\delta = 1.07$ mm/s and $\Delta E_Q = -2.39$ mm/s). The blue lines are simulations with the same parameters, except for the rhombicity E/D, which was changed to 0.16.

that the structure of TauD−{FeNO}^{8} is best characterized by the model ^{3}**H**.

Annealing of TauD−{FeNO}^{8}. We have also explored the reactivity of TauD−{FeNO}^{8} by studying Mössbauer spectra of samples that were annealed after cryoreduction. In general, the low temperature employed during the cryoreduction experiment ($T = 77$ K) prevents significant nuclear rearrangement of the cryoreduced species; that is, the latter is trapped in the geometry that is similar or identical to that of the cluster in the oxidized state. Annealing of a cryoreduced sample (i.e., exposure of that sample to an elevated temperature for some time) may then allow for relaxation of the cluster from its nonequilibrium geometry. In many cases, this process entails the transfer of a proton to the cluster to balance the charge. An example for this type of reactivity is the cryoreduction and annealing of the oxo-bridged nonheme-diiron(III/III) cluster of hemerythrin, for which protonation of the oxo-bridge of the cryoreduced, diiron(II/III) cluster was observed.[54] Other reactions may also occur. An example is the cryoreduction of the oxo-bridged nonheme-diiron(III/III) cluster of *E. coli* ribonucleotide reductase R2 subunit. It is believed that the cryoreduced, oxo-bridged

(53) Zein, S.; Duboc, C.; Lubitz, W.; Neese, F. *Inorg. Chem.* **2008**, *47*, 134–142.

(54) Davydov, R.; Kuprin, R.; Gräslund, A.; Ehrenberg, A. *J. Am. Chem. Soc.* **1994**, *116*, 11120–11128.

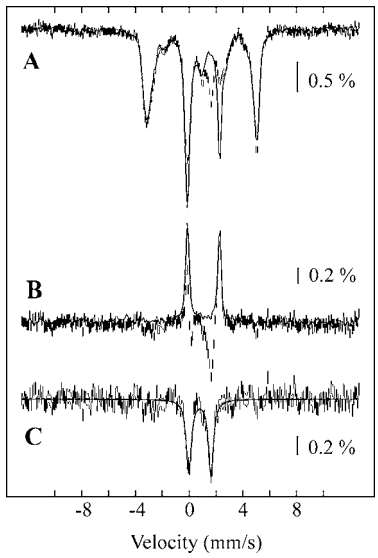

Figure 14. Annealing of TauD−{FeNO}^{8} monitored by Mössbauer spectroscopy: 4.2 K/53 mT Mössbauer spectra of a cryoreduced sample of TauD:Fe(II):αKG:taurine, which was treated with NO, recorded before (solid line) and after (vertical bars) annealing of the sample at 193 K for 2 min (A); difference spectrum between the two spectra shown in (A) (vertical bars) and the reference spectrum of TauD−{FeNO}^{8} (solid line, 17% of total intensity pointing upward) (B); and reference spectrum for annealed TauD−{FeNO}^{8} (vertical bars) and simulation thereof to a quadrupole doublet with the following parameters: $\delta = 0.80$ mm/s and $|\Delta E_Q| = 1.64$ mm/s, 16% of total intensity, solid line (C).

diiron(II/III) undergoes a carboxylate shift, that is, rearrangement and change of the binding mode of one or more carboxylate ligands.[55]

Exposure of a sample containing TauD−{FeNO}^{8} for 2 min at 193 K results in a decrease in the intensity of the high energy line of the TauD−{FeNO}^{8} quadrupole doublet (Figure 14A, solid line) at the expense of a new line at ∼1.6 mm/s (Figure 14A, vertical bars). Adding back 17% of the reference spectrum of TauD−{FeNO}^{8} (Figure 14B, solid line) to the difference spectrum of the above two spectra (Figure 14B, vertical bars) unveils the features of the new species formed upon annealing (Figure 14C, vertical bars). This spectrum can be simulated with a quadrupole doublet with $\delta = 0.80$ mm/s and $\Delta E_Q = 1.64$ mm/s (17% of total intensity).

The experimentally observed parameters are in good agreement with those calculated for the quintet structures of the {FeHNO}^{8} complex, ^{5}**E**H and ^{5}**F**H (Table S2). The corresponding triplet and septet structures of {FeHNO}^{8} are ruled out as possible candidates for annealed TauD−{FeNO}^{8}, because their calculated parameters deviate from the experimental values more than the typical uncertainty of the methodology. Thus, the calculations suggest that annealing of TauD−{FeNO}^{8} results in protonation of this complex and at the same time a spin-crossover may occur eventually yielding a quintet TauD−{FeHNO}^{8} species. The quintet {FeHNO}^{8} species may best be interpreted as a high-spin ferric center ($S_{Fe} = 5/2$) that is antiferromagnetically coupled to a monoanionic HNO$^-$ radical ($S_{HNO} = 1/2$) (Figure S8), while the corresponding triplet species are best described as an intermediate-spin Fe(III) ($S_{Fe} = 3/2$) bound to an HNO$^-$ radical ($S_{HNO} = 1/2$) in an antiferromagnetic fashion (Figure S9). The change of the ground-state spin multiplicity of TauD−{FeHNO}^{8} may be rationalized by the fact that an intermediate-spin state is disfavored by the weak ligand field of typical nonheme-iron active sites such as that found in TauD. In fact, the B3LYP calculations predict the quintet species to be ∼4 kcal/mol lower in energy than the triplet state (Table S1).

Discussion

In the present work, the electronic structures of the quartet TauD−{FeNO}^{7} complex and its one-electron reduced species TauD−{FeNO}^{8} were investigated by a combined experimental and theoretical approach in an effort to reach experimentally calibrated bonding schemes. The {FeNO}^{8} species is of particular interest, because it is isoelectronic with the elusive {FeO$_2$}^{8} species, presumably a key intermediate in the reaction cycle of TauD that has thus far escaped experimental characterization. In accordance with previous studies on model compounds and nonheme iron proteins,[22a] the quartet {FeNO}^{7} species may best be rationalized by a high-spin ferric ion ($S_{Fe} = 5/2$) antiferromagnetically coupled to a triplet NO$^-$ ($S_{NO} = 1$) ligand, thus yielding a quartet ground state. The antiferromagnetic coupling is described by two coupling pathways: the σ-pathway involving the Fe-d_{xz} and NO-π^*_{ip} orbitals and the π-pathway consisting of the Fe-d_{yz} and NO-π^*_{op} orbitals. The coupling strength should be rather strong as evidenced by the large mutual overlaps of the magnetic orbitals in each pathway. In fact, the calculated exchange coupling constant has the magnitude of ∼2000 cm^{-1}. This may be traced back to the substantial metal contributions to the essentially NO-based MOs and vice versa via significant charge donation and backbonding of the NO ligand, respectively. In other words, the derived bonding scheme reflects the highly covalent nature of the bonding between the iron center and the NO$^-$ ligand.

According to the experimental results, it can be stated with certainty that TauD−{FeNO}^{8} is a paramagnetic species. However, its ground-state spin multiplicity could not be unambiguously determined from experiment alone. To the best of our knowledge, this TauD−{FeNO}^{8} is thus far the first case of a paramagnetic {FeNO}^{8} species. Hence, all possible spin states ($S = 1, 2, 3$) were taken into account in the theoretical calculations on this species. The analysis of the electronic structures of all TauD−{FeNO}^{8} models constructed in this work reveals that reduction is invariably a metal-centered process leading to a high-spin ferrous center. This is consistent with the Mössbauer results. From an energetic point of view, the triplet species is the most likely candidate for the trapped TauD−{FeNO}^{8} intermediate. The bonding is best described by antiferromagnetic coupling of a high-spin ferrous center ($S_{Fe} = 2$) and a triplet NO$^-$ ligand ($S_{NO} = 1$). By comparison, the one-electron reduction of [(cyclam-ac)Fe(NO)]$^+$ ({FeNO}^{7}, $S = 1/2$) is found to be a ligand-based process.[46] The difference may be traced back to the different electronic structures of the parent {FeNO}^{7} species. In [(cyclam-ac)Fe(NO)]$^+$ ($S = 1/2$), a low-spin ferrous center ($S_{Fe} = 0$) is bound to an NO$^\bullet$ radical ($S_{NO} = 1/2$), while TauD−{FeNO}^{7} contains a high-spin ferric ion ($S_{Fe} = 5/2$) that is antiferromagnetically coupled to an NO$^-$ ligand ($S_{NO} = 1$). If the redox process took place primarily on the metal center in [(cyclam-ac)Fe(NO)]$^+$, the extra electron would enter into a strongly σ-antibonding e_g orbital, because the t_{2g} subshell of the low-spin ferrous center is completely filled. As a consequence, an NO-centered reduction is the preferred outcome for [(cyclam-ac)Fe(NO)]$^+$. By contrast, the extra electron enters into the essentially nonbonding or weakly

(55) Krebs, C.; Davydov, R.; Baldwin, J.; Hoffman, B. M.; Bollinger, J. M., Jr.; Huynh, B. H. *J. Am. Chem. Soc.* **2000**, *122*, 5327–5336.

π-antibonding t_{2g}-derived orbital of the high-spin ferric center in TauD−{FeNO}^{7}, making a metal-centered reduction preferable over a ligand-based reduction, because the electron affinity of anionic NO^- is substantially lower than that of its one-electron oxidized form $NO^\bullet$. If it were an NO-based reduction, the extra electron would reside in the antibonding MO that consists of the Fe-d_{xz} and NO-π^*_{ip} or the Fe-d_{yz} and NO-π^*_{op} fragment orbitals in the spin-up manifold. Thus, one may readily appreciate that the latter scenario is unlikely due to the unfavorable energy.

The present study serves as an example for how powerful the combination of spectroscopy and theory is. Considering the experimental Mössbauer spectra of TauD−{FeNO}^{8} alone, it is not possible to obtain a unique set of parameters. The spectroscopic parameters calculated for the various model structures serve as a good starting point for spectral simulations. Surprisingly, although these simulations depend on 14 parameters, a satisfactory solution can be obtained by changing only one of the computationally predicted parameters, the one with the largest theoretical uncertainty, the rhombicity *E*/*D*. Conversely, this approach also allows one to rule out hypothetical structures, if their predicted spectroscopic parameters are incompatible with the experimental results, despite the fact that the total energy of such models may not lead to such a conclusion, as is observed for the two triplet models of TauD−{FeNO}^{8}, which have a comparable total energy.

The reactivity of the trapped {FeNO}^{8} species is significantly different from that for {FeO_2}^{8}. Work by Solomon and co-workers[22b] proposed that the latter species is best described as a high-spin Fe(III) ($S_{Fe} = 5/2$) antiferromagnetically coupled to a superoxide, $O_2^{-\bullet}$ ($S_{O2} = 1/2$). Our work revealed that the electronic structure of the {FeNO}^{8} moiety is distinct, presumably leading to a diverging reaction outcome. The reaction mechanism of the Fe(II)- and αKG-dependent dioxygenases has been studied by DFT calculations.[56] In the optimized structure of the quintet {FeO_2}^{8} species, the O_2 ligand is situated above the carbonyl group of αKG with a short distance (2.61 Å) of the distal O atom of O_2 and C2 of αKG. This orientation should facilitate the nucleophilic attack of the oxygen on the C2 atom of αKG to form the proposed bicyclic intermediate **II** (Scheme 1). In the triplet {FeNO}^{8} species, the NO ligand is not situated above the C═O group of αKG; thus, no NO π^* orbitals point toward the C2 atom of αKG. As a consequence, the proposed nucleophilic attack is unlikely to take place, and hence different reaction pathways result. In line with this analysis, a {FeHNO}^{8} species is obtained upon annealing.

(56) Borowski, T.; Bassan, A.; Siegbahn, P. E. M. *Chem.-Eur. J.* **2004**, *10*, 1031–1041.

Conclusion

In the present work, a combined experimental and theoretical study has been performed on the TauD−{FeNO}^{7,8} species. The bonding of both species has been investigated in detail and validated through the successful prediction of the Mössbauer spectroscopic parameters. This allows the description of the quartet TauD−{FeNO}^{7} species as a high-spin ferric ion ($S_{Fe} = 5/2$) antiferromagnetically bound to an NO^- ($S_{NO} = 1$), in close analogy to the electronic structure developed by Solomon and co-workers for model complexes.[22]

The main body of the investigation is concerned with the elusive paramagnetic TauD−{FeNO}^{8} species that differs fundamentally from the diamagnetic {FeNO}^{8} species characterized in model systems.[46] The paramagnetic {FeNO}^{8} species in TauD is formed by cryoreduction of TauD−{FeNO}^{7}. Many different electronic structures can be envisioned for this species. However, our calculations suggest that the reduction is metal-centered and leads to a triplet {FeNO}^{8} species. The reactivity of this species is distinctly different from the postulated, isoelectronic {FeO_2}^{8} intermediate in the TauD reaction cycle. Rather than attacking the αKG cosubstrate, a {FeHNO}^{8} species appears to be formed upon annealing.

Acknowledgment. We gratefully acknowledge financial support of this work from DFG (DFG-NE 690/7-1 to S.Y., F.N., J.M.B., and C.K.), the NSF (CHE-724084 to F.N., J.M.B., and C.K. and MCB-642058 to J.M.B. and C.K.), and NIH (GM-69657 to J.M.B. and C.K.). We thank Lee M. Hoffart for assistance with the analysis of the Mössbauer spectra and Candace C. Davison from the Breazeale Nuclear Reactor of the Pennsylvania State University for assistance with the cryoreduction experiments.

Supporting Information Available: Tables with geometric and spectroscopic properties of the computed models of the TauD−{FeHNO}^{8} complex; schematic MO diagrams for the computed models of the TauD−{FeHNO}^{8} complex; and simulations of high-field Mössbauer spectra of TauD−{FeNO}^{8} using computationally predicted parameters. This material is available free of charge via the Internet at http://pubs.acs.org.

JA909715G